

MOFs

Prediction of Reactive Nitrous Acid Formation in Rare-Earth MOFs via *ab initio* Molecular Dynamics

Dayton J. Vogel, Jessica M. Rimsza,* and Tina M. Nenoff*

Abstract: Reactive gas formation in pores of metal–organic frameworks (MOFs) is a known mechanism of framework destruction; understanding those mechanisms for future durability design is key to next generation adsorbents. Herein, an extensive set of *ab initio* molecular dynamics (AIMD) simulations are used for the first time to predict competitive adsorption of mixed acid gases (NO_2 and H_2O) and the in-pore reaction mechanisms for a series of rare earth (RE)-DOBDC MOFs. Spontaneous formation of nitrous acid (HONO) is identified as a result of deprotonation of the MOF organic linker, DOBDC. The unique DOBDC coordination to the metal clusters allows for proton transfer from the linker to the NO_2 without the presence of H_2O and may be a factor in DOBDC MOF durability. This is a previously unreported mechanism of HONO formation in MOFs. With the presented methodology, prediction of future gas interactions in new nanoporous materials can be achieved.

Introduction

Chemical separations are necessary to produce everyday products and services used throughout the world and account for about 40% of US industrial energy use.^[1] 80% of worldwide energy production is still generated using fossil fuels.^[2] Chemical separations are needed to treat flue gas streams which can contain parts per million levels of reactive NO_x (NO_2/NO), SO_x , CO_2 acid gases, along with humidity.^[3–5] The presence of acid gas species in flue gas streams contribute to its toxicity. They also present challenges for separation materials since the intrinsic reactivity of acid gas species results in material poisoning and degradation of many

How to cite: *Angew. Chem. Int. Ed.* **2021**, *60*, 11514–11522
International Edition: doi.org/10.1002/anie.202102956
German Edition: doi.org/10.1002/ange.202102956

adsorbents. Material degradation in the presence of acid gases also increases costs as current materials may only be applied once before losing separation capability.

To address these challenges, significant research has focused on a class of nanoporous materials called metal-organic frameworks (MOFs), which have exhibited excellent qualities for chemical separations.^[6–12] MOFs are synthesized through a judicious selection of metal cluster elements and organic linker molecules, enabling targeted framework compositions, pore size, and ligand functional groups. Furthermore, MOF materials can be tailored to contain unique material characteristics for specific chemical environments.

One method for tuning MOF material properties is to choose a metal precursor with new chemical properties. The development of MOF materials synthesized with lanthanide (Ln) and actinide elements provide unique advantages compared to traditional transition metal MOFs.^[13–15] The inclusion of f block elements offer new electronic structures which can result in unique MOF topologies, and novel optical and magnetic properties.

Recently, a new series of rare earth 2,5-dihydroxyterephthalic acid (RE-DOBDC) MOFs have been synthesized with their crystal structure based on the Zr UiO-66 framework.^[16,17] The RE-DOBDC MOFs maintain a similar framework that is approximate to UiO-66 but provide unique chemical and electronic properties attributed to rare earth elements. Previous DFT calculations have also shown consistency with experimentally measured IR spectra when modelled as fully activated materials, mimicking the experimental conditions.^[17,18] The unique electronic structures provided by Ln 4f electrons offer binding properties not exhibited by Zr. Utilization of the RE elements in the MOF metal centre enabled preferential binding of acid gases, such as NO_x and SO_x , to these frameworks.^[19–21] In addition to the selective adsorption of acid gases, this series of RE-DOBDC MOFs have shown to be structurally stable under humid NO_x environments, and both optically and magnetically responsive to NO_x adsorption in humid environments.^[20–23] The responsiveness of the RE-DOBDC MOFs to NO_x adsorption stems from two primary adsorption sites: i) an unsaturated metal centre and ii) the carboxylates on the DOBDC organic linkers. Resulting chemical species in the MOF pore (post-humid NO_x exposure) were experimentally identified as nitrate, nitrite, and nitro functional groups.^[20]

Previously published experimental work identified newly formed gas species and adsorption site competitions in RE-DOBDC MOFs.^[20] However, the effect of species' formation mechanisms or binding on MOF structural stability was not investigated. This is necessary in order to obtain atomic level insight into adsorption mechanisms and processes. Static

[*] Dr. D. J. Vogel
Nanoscale Sciences Department, Sandia National Laboratories
Albuquerque, NM 87185 (USA)

Dr. J. M. Rimsza
Geochemistry Department, Sandia National Laboratories
Albuquerque, NM 87185 (USA)
E-mail: jrimsza@sandia.gov

Dr. T. M. Nenoff
Material, Physical, and Chemical Sciences, Sandia National Laboratories
Albuquerque, NM 87185 (USA)
E-mail: tmnenof@sandia.gov

Supporting information and the ORCID identification number(s) for the author(s) of this article can be found under:
<https://doi.org/10.1002/anie.202102956>.

© 2021 The Authors. Published by Wiley-VCH GmbH. This is an open access article under the terms of the Creative Commons Attribution License, which permits use, distribution and reproduction in any medium, provided the original work is properly cited.

density functional theory (DFT) simulations at 0 K were performed and validated that H₂O is more strongly bound to the RE metal sites than NO_x, which strongly interacts with the DOBDC linkers.^[20] While these previous DFT studies were able to shed some light on the adsorption process, several assumptions were made, including the concentration and binding location of the acid gas molecules in the structure. Furthermore, the simulations were unable to identify possible formation of secondary molecular species (both long lasting and temporary species), the effect of spatial confinement by the organic linkers on adsorption, and the role of temperature. Since MOFs are comprised of flexible organic linkers, material motion and gas-framework interactions influence the separation capability and needs to be considered in investigations of acid gas separation. Ultimately, an understanding of the structure-property relationship between framework composition and durability is required for the design of MOFs toward applications in more complex, caustic environments. Ab initio molecular dynamics (AIMD) simulations enable real world predictions toward that end.

AIMD combines accurate electronic structure calculations found in DFT and large scale classical molecular dynamic (MD) simulations by implementing DFT electronic structure optimizations at each time step along a MD trajectory. AIMD is computationally expensive but is offset by the level of insight into the energy and chemical behaviour of highly interacting gas-MOF environments. This is true especially for systems containing NO_x species which contain an unpaired electron. All calculations are spin unrestricted,^[24] allowing for the spin to be taken into account. Previous AIMD work has been used to predict competitive adsorption and separations of O₂ versus N₂ in M₂(DOBDC),^[25] C6 alkane isomers,^[26] and to describe the mechanisms of adsorption and desorption of H₂O in M₂(DOBDC).^[27] Additionally, AIMD simulations have been applied to identify unique breathing modes found in MOF materials^[28] and hydrogen uptake in MOF-74.^[29] While these works attest to the insight and predictive capabilities of AIMD simulations, previous work has stopped short of application of AIMD to the simulations of complex multicomponent mixed acid gases.

The application of advanced computing simulations, such as AIMD, are required to address the role of how acid gas mixtures react inside the RE-DOBDC MOF pores. Examples of this include studies of the formation of molecular species, binding energies between the acid gas species and the framework, and framework compensation for local defects. In particular, identification of chemical by-products in situ is very difficult experimentally given the fast time scales and high number of simultaneous interactions. Using AIMD provides valuable atomistic mechanism information that cannot be achieved otherwise.

To overcome the inherent shortfalls of standard computational investigations we present, for the first time, an AIMD investigation of separation of complex mixed acid gas environments in RE-DOBDC MOFs. To identify the mechanisms that control the interactions of mixed acid gases with RE-DOBDC MOFs, 24 unique dynamic AIMD simulations were performed for both single gas adsorption of NO₂ and H₂O and mixed gas compositions of NO₂ and H₂O in RE-

DOBDC MOFs (RE = Eu, Tb, Y, Yb) at ambient temperatures. The suite of AIMD simulations enabled the exploration of the effect of acid gas composition and concentration on the in-pore formation of various nitrous biproducts. These simulations enable the first computational investigation of this novel and stable RE-DOBDC MOF series in response to complex mixed acid gas environments, with the results providing mechanistic-based insights that can be used to predict the material response to even more complex acid gas mixtures.

Additionally, detailed analysis focuses on the interaction between the RE-DOBDC MOF framework and NO₂ adsorbed gas molecules. Previous experimental results had identified multiple unique reactions occurring between humid NO_x and RE-DOBDC MOFs including interaction between NO_x and the DOBDC linker.^[20] NO₂ adsorption or desorption at unsaturated RE metal sites, reactions between NO₂-DOBDC hydroxyl linkers, C-NO₂ nitro formation, N₂O₄ formation, and HONO formation were all explored. The formation of HONO is highlighted as it is an important precursor to the hydroxyl radical, which is detrimental in atmospheric chemistry.^[30] Furthermore, HONO has also been shown to reactively interact with UiO-66-NH₂ MOFs, resulting in HONO being broken down into N₂ and H₂O.^[31]

The application of AIMD allows for the simulation of spontaneous reactions between in-pore acid gas molecules, and between the acid gas molecules and the MOF framework. Through this complex AIMD simulation series, the preponderance of HONO formation and its bonding to MOF frameworks is highlighted. Additionally, unique chemical insights are presented from more realistic temperature affects as compared with static DFT calculations. Importantly, the use of AIMD enables the future design of novel and optimized nanoporous materials for selective adsorption and durability to more complex and industrially relevant acid gas stream.

Results and Discussion

The application of AIMD allows for the simulation of spontaneous reactions between individual acid gas molecules inside the MOF pore, and between the acid gas molecule and the MOF framework. The results allow for the evaluation of competitive adsorption between NO₂ and H₂O at both the unsaturated metal centres and the DOBDC linkers. Pure and binary mixtures of H₂O and NO₂ were evaluated for identification of how competitive effects may impact adsorption and separation. The complete data set of acid gas adsorption for all 24 structures are included in the SI (Tables S1,S2).

Selection of acid gas mixtures

A total of 24 unique AIMD trajectories were designated as vital to determining the effects of MOF metal centre choice, gas selectivity in adsorption, including gas composition, gas pressure, and adsorption temperature. First, four different metal centres (RE = Eu, Tb, Y, Yb) of the RE-

DOBDC MOF were evaluated to identify their influence on adsorption. Next, single gas compositions were simulated for H₂O and NO₂ as a benchmark for comparing with more complex gas mixtures. Binary gas mixtures (H₂O:NO₂) were then simulated to identify direct competitive effects between two different acid gases. The increase in complexity of the gas mixtures allows for the simulation of competitive effects between gas species in adsorption behaviour. The final variable was gas concentration, with both low and high concentrations of each gas mixture being simulated (i.e. 1 NO₂ molecule versus 12 NO₂ molecules, 1:1 H₂O:NO₂ versus 6:6 H₂O:NO₂). The ratio and composition of acid gases simulated in all AIMD trajectories are included in Table 1. The RE-DOBDC MOF structures contain 12 metal atoms in the unit cell, therefore a maximum of 12 acid gas molecules were included in the simulation. This enabled gas adsorption at 100% of the metal sites. The complete data set of acid gas adsorption for all 24 trajectories is included in the SI (Tables S1,S2) and an example RE-DOBDC structure is included in Figure 1.

Table 1: Ratio and acid gas species for all AIMD trajectories in Eu, Tb, Y, and Yb -DOBDC MOFs.

Rare-Earth Metal	Number of Gas Molecules	Gas Composition
Eu, Tb, Y, Yb	1	H ₂ O or NO ₂
Eu, Tb, Y, Yb	12	H ₂ O or NO ₂
Eu, Tb, Y, Yb	2	1 H ₂ O:1 NO ₂
Eu, Tb, Y, Yb	12	6 H ₂ O:6 NO ₂

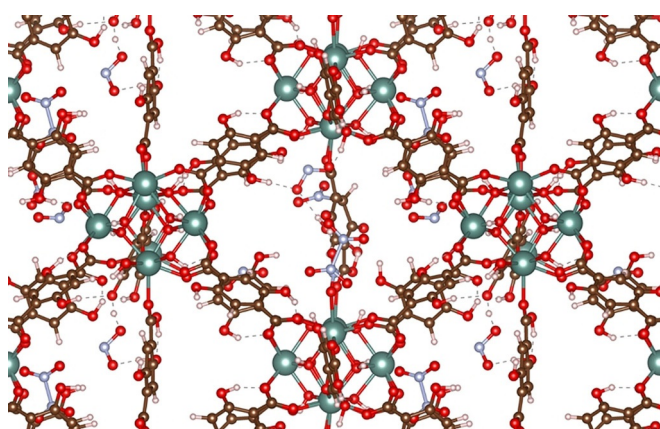


Figure 1. Image of Y-DOBDC + 12 NO₂ comprised of multiple calculation unit cells to show MOF structure and coordination. Dotted lines show H-bonding. Y (green), O (red), C (brown), H (white), and N (blue).

Metal dependence of adsorption

Overall, limited variation in adsorption of H₂O and NO₂ at the metal centres in the RE-DOBDC MOFs were hypothesized, based on previously calculated DFT binding energies for H₂O and NO₂ in RE-DOBDC MOFs, which identified that H₂O is bound more strongly than NO₂ across the entire Ln-series.^[32] Additionally, the statically calculated binding energies for H₂O and NO₂ in RE-DOBDC MOFs

reported by Vogel et al.^[32] exhibited only a ≈ 0.1 eV variation in binding energies in RE-DOBDC MOFs. Here, metal centre dependence of adsorption across all AIMD trajectories included 9 total adsorption events at metal centres in the Eu-DOBDC trajectories, 4 in Tb-DOBDC, 6 in Y-DOBDC and 4 Yb-DOBDC, Table S2. Along the calculated AIMD trajectories, adsorption at a RE metal site is classified as gas adsorption to a RE atom without desorption. This trend in metal adsorption events closely follows the Ln contraction trend in ionic $3 +$ radii $\text{Eu} > \text{Tb} > \text{Y} > \text{Yb}$ for RE elements.^[33] The decreasing ionic radii size results in a decrease in unit cell size and RE-DOBDC MOF pore volume. This places the gas molecules in closer proximity to each other in the pore and increases the number of gas-gas and gas-DOBDC interactions.^[24] Tb shows a lower number of adsorption compared to the smaller Y. However, it can be contributed to the small number of events along the trajectory. Therefore, the trend in gas adsorption indicates that it is the volume of the unit cell, Table S3, and not necessarily the chemistry of the metal centre, that is causing increased metal site adsorption through more frequent competitive interactions.

Gas adsorption dependence on concentration

Gas adsorption at metal sites is the primary mechanism of adsorption in MOF materials and occurs in all AIMD trajectories. When analysing the effects of gas concentration in the RE-DOBDC MOF analogues, comparison of adsorption behaviour between low and high concentration gas mixtures shows a clear distinction. In low gas concentrations containing a single H₂O molecule adsorption at a metal site occurs only in the Y-DOBDC MOF. However, high concentration H₂O gas mixtures (12 H₂O) account for 95% of all identified metal site adsorption events along the AIMD trajectories, Figure 2, with adsorption occurring in the Eu, Tb, Y, and Yb -DOBDC MOFs. At low concentrations, the individual acid gases were observed to interact with the DOBDC linkers, hindering their ability to diffuse to an unsaturated metal site, resulting in minimal adsorption. The

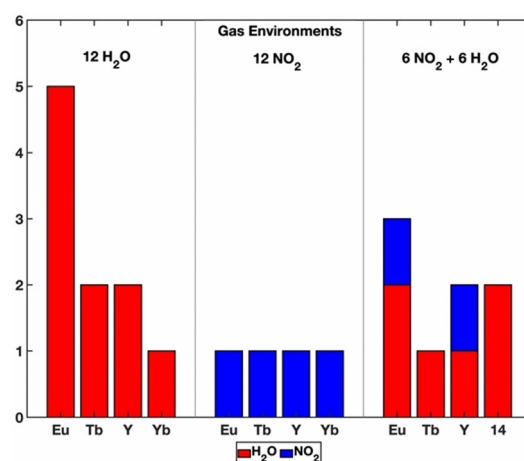


Figure 2. Number of gas adsorption events at unsaturated RE metal sites in RE-DOBDC MOFs in high concentration gas environments of 12 H₂O, 12 NO₂, and 6 NO₂ + 6 H₂O.

formation of new chemical species is also concentration dependent, with increased formation of new chemical species and increased gas adsorption along the AIMD trajectories, Figure 2 and Table S1.

Gas adsorption dependence on composition

Identification of competitive adsorption is investigated through comparisons of high concentration single and binary H₂O and NO₂ gas mixtures. Initially focusing on pure NO₂ gas, limited gas-metal adsorption in the 12 NO₂ trajectories was observed, with a total of 4 adsorption events. The low number of adsorption events highlights the weak adsorption energy of NO₂ at unsaturated metal sites in RE-DOBDC MOFs compared with H₂O or mixed H₂O + NO₂ gases. In comparison to pure NO₂, the 12H₂O trajectories show a total of 9 adsorption events and indicates a stronger interaction of H₂O at the metal sites. This finding is in agreement with previous static DFT calculations in RE-DOBDC MOFs which identified a binding energy trend of H₂O > NO₂ across the RE-DOBDC MOF series at unsaturated metal sites.^[52]

NO₂ is known to adsorb to both metal centres and ligands,^[20] which may be affected through competition with H₂O adsorption. In the binary 6NO₂ + 6H₂O gas mixture, the NO₂ adsorption is reduced compared to pure 12NO₂. In all mixed gas trajectories, NO₂ is the least common molecule bound to a metal centre, accounting for only 25% of the bound species in the 6NO₂ + 6H₂O trajectories, indicating competitive metal site adsorption between NO₂ and H₂O. The new competing interactions are hypothesized as NO₂-H₂O gas-gas interactions and H₂O-metal adsorption. However, as the number of NO₂ adsorption events decreased following the introduction of H₂O into the AIMD trajectories, from 4 to 2, the total number of gas adsorption events at metal centres increased, from 4 to 8. The increased metal site adsorption is due specifically to H₂O adsorption, highlighting the stronger H₂O interaction when directly competing with NO₂. As the H₂O preferentially binds at the metal sites, NO₂ begins to adsorb in a different pore location.

Despite the energetic preference for H₂O adsorption at the metal centre and the high adsorption of NO₂ on the linker, metal site adsorption of NO₂ was still identified. The AIMD trajectories highlighted a series of conditions which allow the NO₂ to adsorb at an unsaturated metal site and are detailed later in this manuscript.

Formation of secondary molecular species in MOFs

In complex gas mixtures, newly formed by-product species play a role in competitive gas-MOF interactions. In studying the effects of competitive gas adsorption, the data shows five new species observed across the AIMD subset: HONO, N₂O₄, nitrate groups, nitro groups, and H₃O⁺. The new individual molecular species N₂O₄ is formed via 2NO₂ ⇌ N₂O₄, while H₃O⁺ is formed via H₂O deprotonation of a DOBDC hydroxyl, see Scheme S3. The formation mechanisms of new nitrate and nitro groups are provided in Schemes S1, S2, respectively, and the formation of HONO explored in depth later in this manuscript. The total number of MOF-NO₂

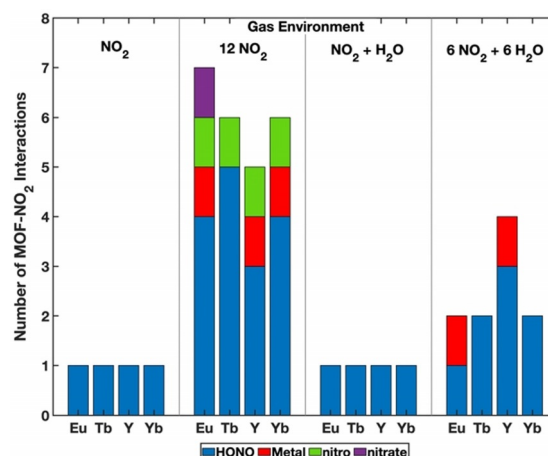


Figure 3. The total number of strong MOF-NO₂ interactions are presented for Eu, Tb, Y, and Yb -DOBDC in acid gas environments containing NO₂: NO₂, 12NO₂, NO₂ + H₂O, and 6NO₂ + 6H₂O. The number of new HONO species (blue), NO₂ adsorbing to a metal site (red), nitrate formation (purple), and nitro formation (green) are presented for each RE element of the RE-DOBDC MOF, in the respective gas environments.

interactions are presented for Eu, Tb, Y, and Yb -DOBDC in four acid gas environments: NO₂, 12NO₂, NO₂ + H₂O, and 6NO₂ + 6H₂O in Figure 3.

The most reactive gas species identified in the AIMD trajectories was NO₂, as it was calculated to adsorb at metal sites and resulted in by-product species within the RE-DOBDC MOFs. In the data set, all of the AIMD trajectories that contained NO₂ resulted in the formation of nitrogen based gas-MOF interactions that were not present the beginning of AIMD trajectories, Figure 3. Adsorption data identifies 5NO₂ binding events at metal centres, 5NO₂ binding events to ligands, 32HONO molecules formed, 4N₂O₄ molecules formed, 4nitro (R-NO₂) groups formed, and 1nitrate (R-ONO₂) formed across the 4RE-DOBDC MOFs studied.

The formation of a HONO, nitro, or nitrate species in all calculated RE-DOBDC structures indicates a strong interaction of NO₂ with multiple parts of the MOF framework. Specifically, the formation of HONO, nitro, and nitrate all result from a NO₂-DOBDC linker interaction. However, following the introduction of H₂O, the predominance of HONO is slightly reduced and the formation of nitro and nitrate groups are not seen. This indicates a change in how NO₂ interacts with the DOBDC linkers. The changes are hypothesized to be attributed to NO₂-H₂O interactions and H₂O-DOBDC interactions, that can interfere with HONO, nitro, and nitrate formation. The concentrations and mechanism of formation of these by-products are discussed in detail below.

Identification of NO₂ interactions with the MOF

As previously stated, the strong NO₂-DOBDC interactions allow for the formation of new chemical species, including new N-O or N-C chemical bonds in the RE-DOBDC pore. The formation of N-O bonds can occur at the

DOBDC anchoring carbonyl O atoms or at a DOBDC hydroxyl group, as they are the most available O framework atoms. The interactions with linker O atoms can result in one of two chemical reactions: either the breaking a RE–O bond at an anchoring carbonyl or the deprotonation of a hydroxyl group. New N–C bonds are created during the formation of nitro groups, which forms a N–C bond between the N of NO₂ and an alpha carbon relative to the DOBDC hydroxyl group, Scheme S2.

The formation of new N bonds, specifically N–O bonds, indicate the reactive effects of MOF-gas interactions within the material. The new functional groups, combined with adsorption of NO₂ at RE metal sites, provide insight into the possible capture of NO₂ in competitive gas environments. Such complex reactions could result in degradation of the MOF and require multiple interactions to occur simultaneously.

HONO formation from NO₂ + H₂O in the MOF framework

The direct comparison between pure NO₂ and pure H₂O in the RE-DOBDC framework showed the formation of HONO occurs more readily in dry NO_x gas environments than with humid NO_x. While HONO can form in both dry and humid environments, H₂O was observed to also interact with DOBDC hydroxyl groups which creates competition at linker sites with NO₂. The interaction of H₂O with DOBDC hydroxyl groups can result in H₃O⁺ formation, Scheme S3, but does not form new bonds with the linker. The effect of humidity is a reduction in the number of interactions NO₂ can experience with DOBDC hydroxyl H atoms. Even accounting for HONO formation, through proton transfer along a chain of water molecules, does not offset the ability for NO₂ to deprotonate the DOBDC linker. The spontaneous formation of HONO exemplifies the NO₂-MOF interaction found within RE-DOBDC MOFs. However, formation of HONO in a dry environment is unique, as known mechanisms for HONO formation involve H₂O.^[34,35] HONO formation has also been identified in atmospheric mixtures of NO₂, SO₂, and H₂O; this is the only known environment which shows favourable formation of HONO with the inclusion of H₂O.^[36]

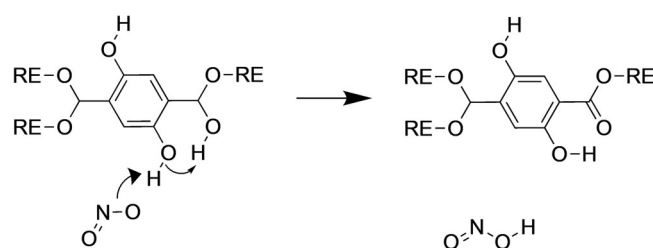
Detailed Analysis of AIMD simulations

The commonality found in the HONO formation of RE-DOBDC MOFs indicates this is a predominant occurrence. The mechanisms of HONO formation are essential to reactive gas species formation in MOFs. This chemical reaction has never been observed experimentally in RE-DOBDC MOFs and is only isolated through the power of AIMD simulations. Therefore, a deep dive into the simulation results is necessary to understand mechanisms of formation that can be applied in future material design. Below is a detailed accounting of the mechanistic results of AIMD simulations and analyses of (i) HONO formation, (ii) HONO formation conditions, (iii) NO₂ adsorption in an exemplar RE-DOBDC MOF (RE = Y), and (iv) the formation of secondary nitrogen species.

(i) AIMD simulations for a step by step formation timeline of HONO formation

Mechanisms of HONO formation in RE-DOBDC MOFs were found to occur primarily via the binding to a monodentate DOBDC hydroxyl group. Published RE-DOBDC crystal data identified two linker coordinations, monodentate and bidentate, at 33% and 67% in the original unit cell, respectively.^[16] The coordination is indicative of native defect sites in MOF materials,^[18,37] which can be formed due to crystallization kinetics and allows both linker coordinations to exist, Scheme S4. The defect allows for a more flexible coordination within the MOF that can enable metal cluster and linker rotation, known to exist in certain MOFs.^[38,39] The monodentate linkers also result in an extra hydroxyl group on one third of the organic linkers in RE-DOBDC MOFs, which serve as reactive sites in the material.

From the AIMD trajectories, it was observed that as NO₂ approaches the hydroxyl group of a monodentate linker, a strong hydrogen bonding interaction forms. The H atom of the hydroxyl then begins to transfer between the NO₂ and the hydroxyl O atom. While all DOBDC linkers have hydroxyl groups, it is the extra neighbouring hydroxyl group found only on monodentate coordination which assists in the formation of HONO. The neighbouring hydroxyl allows a H to be shared between two hydroxyl groups, allowing NO₂ to take the H and form HONO, Scheme 1.



Scheme 1. Mechanism of HONO formation via NO₂ interacting with a monodentate DOBDC hydroxyl group, facilitated by neighbouring hydroxyl.

The transfer of a DOBDC hydroxyl H atom can also occur in two less frequent mechanisms. In the first mechanism, a bidentate coordinated linker can produce HONO following a specific mechanism in which an NO₂ interacts with the DOBDC hydroxyl group and a second NO₂ molecule approaches the O to form a nitrate or provide a H atom, Scheme S1. In both cases of H removal from the linker, a secondary interaction is provided to assist the mechanism. In the second mechanism, a H₂O deprotonates the linker and then transfers the H atom to a nearby NO₂. The resulting HONO molecular formations include all isomers of the molecule: *trans*-HONO, *cis*-HONO, and isonitrous acid (HNO₂),^[40] with the *trans*-HONO molecule as the primary isomer. The distribution of the HONO isomers is included in Figure S1. The frequent generation of HONO species across the majority of trajectories identifies the strength of interaction in highly competitive environments. It was hypothesized and validated that NO₂ interacts with the DOBDC

linker, but the identification of new HONO products, compared to nitro and nitrate formation, is a new mechanism not formerly identified.

The new species formed from strong NO_2 interactions are identified for all RE metals simulated. As previously stated, there is no clear trend between strong NO_2 interactions and the RE metal in the MOF. Given the non-metal dependent relationship, as well as established similarity in adsorption across the Ln series, the Y-DOBDC material has been chosen for use in an exemplary trajectory for in depth analysis. The identification and analysis of NO_2 interactions in Y-DOBDC are expected to be representative for the same interactions in all RE-DOBDC MOFs.

(ii) AIMD analysis of HONO formation conditions

The primary HONO formation mechanism is identified to be a NO_2 molecule deprotonating a monodentate bound DOBDC hydroxyl, as shown in Scheme 1. The atoms and bonds of the NO_2 and DOBDC hydroxyl are presented in Figure 4.

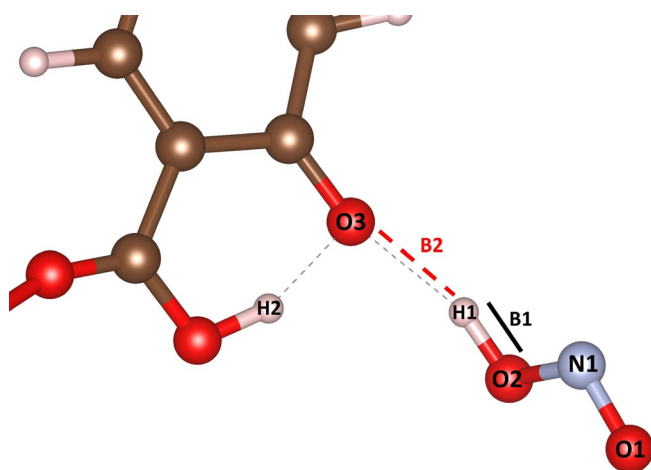


Figure 4. Formation of HONO via interaction of an NO_2 and monodentate DOBDC linker. C (brown), N (light blue), O (red), and H (white). The bond lengths of O2-H, B1, and H1-O3, B2, are compared to determine HONO formation.

A HONO molecule containing N1, O1, O2, and H1 is shown interacting with a previously deprotonated DOBDC hydroxyl O atom, O3. As the bond between the NO_2 and H1 (B1) reaches 1 \AA , the HONO molecule is formed. The originally deprotonated O atom (O3) is protonated. This proton comes from a neighbouring hydroxyl group, which is only available on monodentate coordinated DOBDC linkers and identifiable via AIMD.

Determination of when the HONO species forms are identified through calculated interatomic distances, Figure 5. At the beginning of the trajectory, the HONO H atom transfers from the original DOBDC hydroxyl group near time 0.18 ps, as seen in Figure 5. The red and blue H-O bond distances in Figure 5 correspond to the B1 and B2 bonds visualized in Figure 4, respectively. Note that in the snapshot of Figure 4, the deprotonated hydroxyl O (O3) has a strong

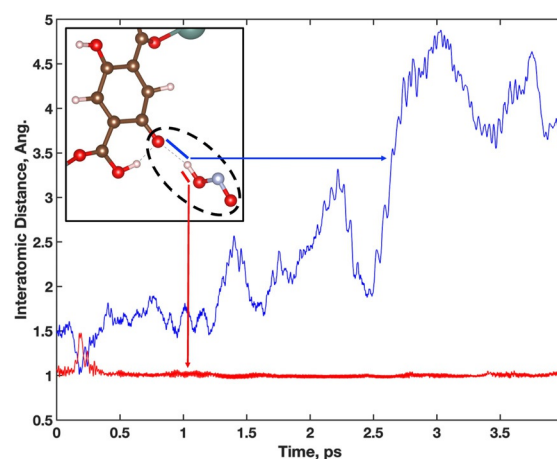


Figure 5. Interatomic distance of H atom between DOBDC hydroxyl group (blue) and NO_2 molecule (red) during the formation of HONO. H (white), C (brown), O (red), Y (teal), N (light blue).

interaction with a neighbouring DOBDC hydroxyl group. This is possible due to the intrinsic defect in the RE-DOBDC materials where the anchoring carboxyl O atoms do not all coordinate to metal sites.

After 0.25 ps, the H atom maintains the expected bond distance of $\approx 1 \text{ \AA}$ with the NO_2 molecule (red), completing the formation of the HONO molecule. After the formation of HONO is complete at 0.25 ps, the atomic distances in Figure 5 (blue) corresponds to the relative distance between the HONO molecule and the deprotonated DOBDC hydroxyl group. The calculated distances range between $1.5\text{--}4.8 \text{ \AA}$ as the HONO molecule moves away from the DOBDC. The distances are subsequently used to identify the relationship between interaction energy and distance of the formed HONO molecule. The interaction energy of the HONO molecule within the system was calculated for two time periods along the trajectory from 0–0.5 ps and 2.2–2.8 ps. These two segments of the trajectory capture the energy of the final H transfer between the DOBDC linker and NO_2 and the HONO molecule dissociating from the deprotonation site.

In the 0–0.5 ps trajectory segment, the HONO molecule is formed both from 0–0.125 ps and again from 0.375–0.5 ps. The average calculated binding energies of HONO with the deprotonated site for these time steps are -0.86 eV and -0.65 eV , respectively. The calculation of time dependent binding energies is defined in the SI. The decreased interaction strength of the HONO with the framework is highly dependent on the distance from the deprotonation site. For example, the average distance from the deprotonated O grows from 1.51 \AA in the 0–0.125 ps range to 1.66 \AA in the 0.375–0.5 ps range. As the HONO molecule finalizes its dissociation from the deprotonation site in 2.6–2.8 ps, the interaction energy weakens to an average of -0.47 eV . The calculated time dependent binding energy of the HONO molecule shows an increase as the time approaches 2.8 ps. However, this is due to the HONO beginning to interact with a new part of the MOF pore. In using the time dependent interaction energies from the final formation of HONO at 3.75 ps to the final dissociation near 2.8 ps, the change in energy is $\approx 0.2 \text{ eV}$. Near 0.2 eV the interaction can be

classified as physisorption of a HONO molecule with the MOF framework. Otherwise, the average total energy during the final formation of the HONO species changes by -0.2 eV, indicating a stability of the HONO formation.

(iii) AIMD simulations of NO_2 adsorption in Y-DOBDC

The first spontaneous reaction analysed along the Y-DOBDC + 12NO_2 AIMD trajectory is desorption at an unsaturated Y metal site.

Examination of a singular NO_2 molecule that experiences desorption along the AIMD trajectory, Figure 6, shows three phases associated with the MOF- NO_2 interaction. First, a NO_2 molecule is initially adsorbed to an unsaturated metal site (blue box) and then desorbs into free pore space (green box), seen in Figure 6. The calculated interaction energies of each of the NO_2 locations within the MOF framework is presented in Figure 6, with corresponding snapshots along the AIMD trajectory.

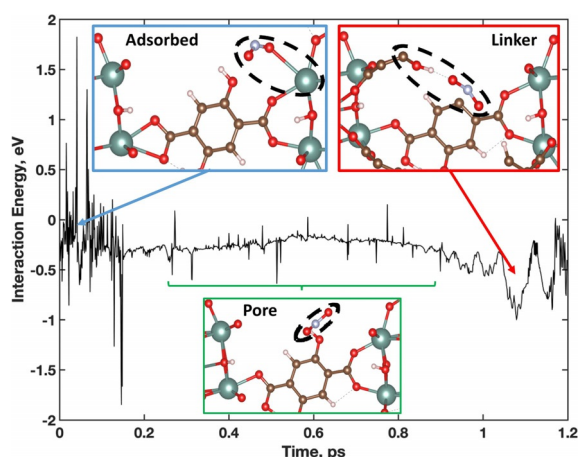


Figure 6. Interaction energy of a NO_2 adsorbed to Y (blue box), desorbed and free in vacuum (green box), and interacting with a DOBDC linker (red box) along the AIMD trajectory. Inset: H (white), C (brown), O (red), Y (teal), N (light blue).

The initial NO_2 adsorption event shows that the NO_2 molecule is in physisorption distance of an unsaturated Y metal site; it does not have any secondary interactions with neighbouring linkers or gas molecules. As the NO_2 desorbs off the MOF framework and into the pore, the interaction energy weakens. It only strengthens again when it has a new binding interaction with a DOBDC hydroxyl group. As the NO_2 approaches the DOBDC linker, the interaction energy again increases to around -1 eV. Interestingly, this interaction energy of NO_2 with the linker is stronger than the binding energy between NO_2 adsorbed to the metal site.

The inverse of the desorption interaction (adsorption of an NO_2 molecule to an unsaturated metal site) is also identified along the same trajectory. In this adsorption event, an NO_2 molecule interacts with a DOBDC hydroxyl group before adsorbing. Inset snapshots along the AIMD trajectory are presented in Figure 7, along with the corresponding interaction energy.

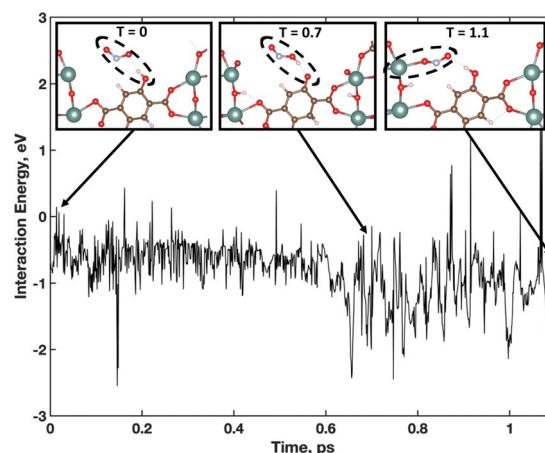


Figure 7. Interaction energy during a NO_2 adsorption event. Inset snapshots of the interaction show three phases: 1) NO_2 /linker 2) proton passing and HONO formation, 3) adsorption to unsaturated metal site. Inset: H (white), C (brown), O (red), Y (teal), N (light blue).

The initial interaction between NO_2 and the hydroxyl group is shown to be in the same energy region, -0.6 to -1.1 eV, as the previously described NO_2 -DOBDC interaction. As the NO_2 nears the DOBDC, a HONO molecule forms 0.7 ps into the interaction with the deprotonation of the DOBDC hydroxyl group. During this interaction, the H atom is transferred back and forth between the NO_2 and DOBDC. As the DOBDC hydroxyl does not have any neighbouring hydroxyl groups which could pass another proton, the NO_2 and DOBDC are reformed and the NO_2 binds at a nearby unsaturated metal site. In this trajectory, the adsorption energy of the NO_2 is stronger than what was calculated for the desorption event. The additional hydrogen bond formed with the adsorbed NO_2 strengthens the NO_2 binding energy.

Prior to permanent NO_2 adsorption at an unsaturated metal site, the following criteria were met: 1) NO_2 hydrogen bonded with DOBDC hydroxyl, 2) no neighbouring hydroxyl group were located nearby to donate a proton, 3) NO_2 was in close proximity to an unsaturated metal, and 4) the continued H-bond interaction formed with the adsorbed NO_2 . These steps have been identified to achieve sustained adsorption. Other NO_2 trajectories were observed to show NO_2 -metal interactions; however, all are short lived and desorbs quickly without any secondary framework interaction.

(iv) AIMD simulations of the formation of the secondary nitrogen species

Species such as nitro, nitrate, and nitrite groups, which form on the DOBDC linkers, were confirmed experimentally by FTIR^[20] and have been identified in current AIMD trajectories. One of them, a nitro group (NO_2) has been further analysed along the Y-DOBDC + 12NO_2 trajectory. Along the first 1 ps of the trajectory, the interaction energy of NO_2 ^[20] has been plotted as with the C–N bond distance, Figure 8.

Initially the NO_2 molecule is located in the MOF pore and ≈ 3.5 Å from the nitro-C atom bond; the average interaction

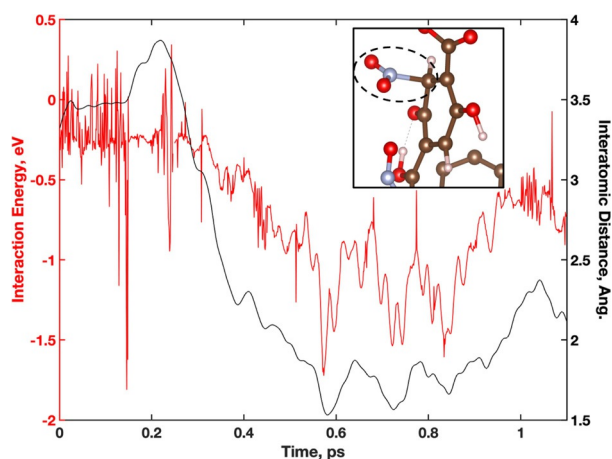


Figure 8. Interaction energy of nitro formation (red) as a function of the C–N bond length (black) along the AIMD trajectory. Inset: H (white), C (brown), O (red), N (light blue).

energy of the NO_2 is approximately -0.15 eV. As the distance of the C–N bond shortens, the interaction energy of the NO_2 with the C strengthens and reaches a value close to -1.5 eV. This interaction energy agrees with the experimental evidence of NO_2 preferring NO_2 -DOBDC interactions as compared to the NO_2 -Ln metal where the energy of adsorption is close to -0.2 eV. What is also of interest in this interaction is the deprotonated state of the DOBDC linker. As can be seen in the inset geometry of Figure 8, the DOBDC hydroxyl group next to the nitro-C has been deprotonated via another gas molecule. Importantly, the deprotonation of the neighbouring hydroxyl is not required for nitro formation but was observed in the majority of cases. The unique interaction of NO_2 binding directly to the MOF DOBDC linkers has previously been identified in M-MOF-74.^[11,12] It was then further confirmed to occur in RE-DOBDC MOFs.^[20] Similar binding was seen in a variety of Zr-based MOFs, which at times resulted in occurrences of material degradation.^[41]

Conclusion

An extensive set of ab initio molecular dynamics (AIMD) simulations were used for the first time to evaluate competitive adsorption of mixed acid gases (NO_2 , H_2O) in a series of RE-DOBDC MOFs. The dynamically evolving trajectories allow for evaluation of spontaneous formation of secondary molecular species in the MOF. These simulations account for the effects of confinement by organic linkers and resulting changes in adsorption that cannot be analysed through static density functional theory (DFT) calculations alone.

Analysis of competitive adsorption identified that the gas composition had a stronger influence on gas adsorption than the specific metal centre (Eu, Tb, Y, Yb). Furthermore, adsorbed H_2O is more frequently bound to metal centres, while NO_2 can bind with both metal centres and the linker. Additionally, the AIMD trajectory identified the formation of secondary molecular species, including HONO, N_2O_4 , nitrate groups, nitro groups, and H_3O^+ .

Of those secondary molecular species formed, the most common is HONO, which is readily formed as a result of deprotonation of the MOF DOBDC organic linker, and not from the interaction between NO_2 and H_2O in the pore space. This is a previously unreported mechanism of HONO formation in MOFs that was discovered, and is reported herein, through this unique application of AIMD methodologies. The unique DOBDC coordination found specifically in RE-DOBDC MOFs allows for proton transfer from the linker to the adsorbed NO_2 without the presence of H_2O . Additionally, several proton transfer events occur prior to HONO formation.

Through the combination of AIMD simulations and validation from previous experiment, unprecedented insight into mechanisms of acid gas separation can be developed not only in MOFs but across porous organic systems. The AIMD simulations provide step-wise improvement in accuracy of computational results including temperature effects and spontaneous reactions. Identification of individual strong MOF-gas interactions in RE-DOBDC MOFs provides fundamental understanding of the separation capability and maintained stability of RE-MOFs under acid gas conditions. Further application of AIMD to simulated mixed acid gas adsorption in MOFs will allow for identification of mechanisms that control competitive adsorption processes with even more complex gas streams. This will also enable future computational design of materials around these adsorption mechanisms.

Acknowledgements

This work was supported as part of UNCAGE-ME, an Energy Frontier Research Center funded by the U.S. Department of Energy, Office of Science, Basic Energy Sciences under Award #DE-SC0012577. Sandia National Laboratories is a multimission laboratory managed and operated by National Technology & Engineering Solutions of Sandia, LLC, a wholly owned subsidiary of Honeywell International Inc., for the U.S. Department of Energy's National Nuclear Security Administration under contract DE-NA0003525. This paper describes objective technical results and analysis. Any subjective views or opinions that might be expressed in the paper do not necessarily represent the views of the U.S. Department of Energy or the United States Government.

Conflict of interest

The authors declare no conflict of interest.

Keywords: ab initio calculations · adsorption · metal-organic frameworks (MOFs) · nitrous acid · rare-earth metals

[1] J. L. Humphrey, G. E. Keller, *Separation Process Technology*, McGraw-Hill, New York, **1997**.

[2] BP, **2020**.

[3] F. Rezaei, A. A. Rownaghi, S. Monjezi, R. P. Lively, C. W. Jones, *Energy Fuels* **2015**, *29*, 5467–5486.

- [4] K. S. Walton, D. S. Sholl, *Joule* **2017**, *1*, 208–211.
- [5] F. Normann, E. Jansson, T. Petersson, K. Andersson, *Int. J. Greenhouse Gas Control* **2013**, *12*, 26–34.
- [6] J.-R. Li, J. Sculley, H.-C. Zhou, *Chem. Rev.* **2012**, *112*, 869–932.
- [7] H. Li, K. Wang, Y. Sun, C. T. Lollar, J. Li, H.-C. Zhou, *Mater. Today* **2018**, *21*, 108–121.
- [8] J.-R. Li, R. J. Kuppler, H.-C. Zhou, *Chem. Soc. Rev.* **2009**, *38*, 1477–1504.
- [9] M. V. Parkes, D. F. Sava Gallis, J. A. Greathouse, T. M. Nenoff, *J. Phys. Chem. C* **2015**, *119*, 6556–6567.
- [10] Z. Zhang, Y. Zhao, Q. Gong, Z. Li, J. Li, *Chem. Commun.* **2013**, *49*, 653–661.
- [11] K. Tan, S. Zuluaga, Q. Gong, Y. Gao, N. Nijem, J. Li, T. Thonhauser, Y. J. Chabal, *Chem. Mater.* **2015**, *27*, 2203–2217.
- [12] K. Tan, S. Zuluaga, H. Wang, P. Canepa, K. Soliman, J. Cure, J. Li, T. Thonhauser, Y. J. Chabal, *Chem. Mater.* **2017**, *29*, 4227–4235.
- [13] E. A. Dolgoplova, A. M. Rice, N. B. Shustova, *Chem. Commun.* **2018**, *54*, 6472–6483.
- [14] S. Fordham, X. Wang, M. Bosch, H.-C. Zhou in *Lanthanide Metal-Organic Frameworks* (Ed.: P. Cheng), Springer Berlin Heidelberg, Berlin, **2015**, pp. 1–27.
- [15] V. Borovkov, *Front. Chem.* **2015**, *3*, 0050.
- [16] D. F. Sava Gallis, L. E. S. Rohwer, M. A. Rodriguez, M. C. Barnhart-Dailey, K. S. Butler, T. S. Luk, J. A. Timlin, K. W. Chapman, *ACS Appl. Mater. Interfaces* **2017**, *9*, 22268–22277.
- [17] D. F. Sava Gallis, J. A. Harvey, C. J. Pearce, M. G. Hall, J. B. DeCoste, M. K. Kinnan, J. A. Greathouse, *J. Mater. Chem. A* **2018**, *6*, 3038–3045.
- [18] J. A. Harvey, J. A. Greathouse, D. F. Sava Gallis, *J. Phys. Chem. C* **2018**, *122*, 26889–26896.
- [19] F. Rezaei, C. W. Jones, *Ind. Eng. Chem. Res.* **2013**, *52*, 12192–12201.
- [20] D. F. Sava Gallis, D. J. Vogel, G. Vincent, J. M. Rimsza, T. M. Nenoff, *ACS Appl. Mater. Interfaces* **2019**, *11*, 43270–43277.
- [21] S. E. Henkelis, D. L. Huber, D. J. Vogel, J. M. Rimsza, T. M. Nenoff, *ACS Appl. Mater. Interfaces* **2020**, *12*, 19504–19510.
- [22] S. E. Henkelis, D. Rademacher, D. J. Vogel, N. R. Valdez, M. A. Rodriguez, L. E. S. Rohwer, T. M. Nenoff, *ACS Appl. Mater. Interfaces* **2020**, *12*, 22845–22852.
- [23] D. J. Vogel, T. M. Nenoff, J. M. Rimsza, *ACS Appl. Mater. Interfaces* **2020**, *12*, 4531–4539.
- [24] D. J. Vogel, D. F. Sava Gallis, T. M. Nenoff, J. M. Rimsza, *Phys. Chem. Chem. Phys.* **2019**, *21*, 23085–23093.
- [25] M. V. Parkes, J. A. Greathouse, D. B. Hart, D. F. Sava Gallis, T. M. Nenoff, *Phys. Chem. Chem. Phys.* **2016**, *18*, 11528–11538.
- [26] H. Wang, X. Dong, J. Lin, S. J. Teat, S. Jensen, J. Cure, E. V. Alexandrov, Q. Xia, K. Tan, Q. Wang, D. H. Olson, D. M. Proserpio, Y. J. Chabal, T. Thonhauser, J. Sun, Y. Han, J. Li, *Nat. Commun.* **2018**, *9*, 1745.
- [27] Y. Li, X. Wang, D. Xu, J. D. Chung, M. Kaviani, B. Huang, *J. Phys. Chem. C* **2015**, *119*, 13021–13031.
- [28] L. Chen, J. P. S. Mowat, D. Fairen-Jimenez, C. A. Morrison, S. P. Thompson, P. A. Wright, T. Düren, *J. Am. Chem. Soc.* **2013**, *135*, 15763–15773.
- [29] P. Suksaengrat, V. Amornkitbamrung, P. Srepusharawoot, R. Ahuja, *ChemPhysChem* **2016**, *17*, 879–884.
- [30] C. Jia, S. Tong, W. Zhang, X. Zhang, W. Li, Z. Wang, L. Wang, Z. Liu, B. Hu, P. Zhao, M. Ge, *Sci. Total Environ.* **2020**, *735*, 139317.
- [31] D. T. McGrath, M. D. Ryan, J. J. MacInnis, T. C. VandenBoer, C. J. Young, M. J. Katz, *Chem. Sci.* **2019**, *10*, 5576–5581.
- [32] D. J. Vogel, Z. R. Lee, C. A. Hanson, S. E. Henkelis, C. M. Smith, T. M. Nenoff, D. A. Dixon, J. M. Rimsza, *J. Phys. Chem. C* **2020**, *124*, 26801–26813.
- [33] B. Cordero, V. Gómez, A. E. Platero-Prats, M. Revés, J. Echeverría, E. Cremades, F. Barragán, S. Alvarez, *Dalton Trans.* **2008**, 2832–2838.
- [34] F. Sakamaki, S. Hatakeyama, H. Akimoto, *Int. J. Chem. Kinet.* **1983**, *15*, 1013–1029.
- [35] F. Spataro, A. Ianniello, *J. Air Waste Manage. Assoc.* **2014**, *64*, 1232–1250.
- [36] Z. Wang, C. Zhang, G. Lv, X. Sun, N. Wang, Z. Li, *Int. J. Mol. Sci.* **2019**, *20*, 3746.
- [37] A. K. Cheetham, T. D. Bennett, F.-X. Coudert, A. L. Goodwin, *Dalton Trans.* **2016**, *45*, 4113–4126.
- [38] S. Pakhira, *RSC Adv.* **2019**, *9*, 38137–38147.
- [39] A. Gonzalez-Nelson, F.-X. Coudert, M. A. van Der Veen, *Nanomaterials* **2019**, *9*, 330.
- [40] R. Asatryan, J. W. Bozzelli, J. M. Simmie, *Int. J. Chem. Kinet.* **2007**, *39*, 378–398.
- [41] A. M. Ebrahim, B. Levasseur, T. J. Bandoz, *Langmuir* **2013**, *29*, 168–174.

Manuscript received: February 27, 2021

Accepted manuscript online: March 10, 2021

Version of record online: April 8, 2021